Setup of evolution equations for two cylindrical vortex sheets

Roman Wowk

Undergraduate Honors Thesis
Supported by National Science Foundation funded REU
Advisor: Prof. Monika Nitsche, University of New Mexico

The evolution of a single cylindrical vortex sheet has been previously explored (Nitsche, 2000). When a second identical vortex sheet is introduced, the initial fluid flow condition cannot be found analytically, and the symmetry that is present with only one vortex sheet is lost. The initial condition for two cylindrical vortex sheets must be found computationally. The evolution equations also require correction factors and regularization in order to be useful. This paper explores the process of setting up the evolution equations and gives preliminary results.

Introduction

A cylindrical vortex sheet is a zero-thickness model for the shear layer that would exist immediately after "dissolving" a hollow cylinder immersed in potential flow that is steady with time. The fluid inside the cylinders would be stationary. For this particular problem, two hollow cylinders would be placed side-by-side, with their axes parallel. The flow in the dimension along the cylinders' axes of symmetry will remain zero, thus reducing the problem to 2-dimensions. The equations that govern the motion of the vortex sheets along with the initial condition, will be introduced in this paper. The evolution equations are then discretized using N point-vortex elements that are initially equally-spaced. The initial condition and the evolution equations will be also nondimensionalized. Due to the use of principal value integrals, corrections factors using Taylor series will be given, as well as a regularization procedure to desingularize the problem. Preliminary results of the vortex sheet evolution will be given.

1. Flow Conditions

The basis for this problem is the Cartesian coordinate system (x,y,z). The fluid velocity is nonzero in the x, and y directions, and is always zero in the z-direction. Therefore, this problem can be solved in a 2-dimensional plane. The initial velocity inside the cylinders is zero, and the velocity at infinity is prescribed. The analytical solution for the potential flow condition around two separated hollow cylinders (side-by-side) is not known, and therefore an approximation must be computed numerically. This will be developed in the following sections. The fluid velocity is defined as

$$\bar{u} = (u, v, 0) \tag{1.1}$$

and the complex velocity is defined as

$$f(x+iy) = u - iv \tag{1.2}$$

The vorticity is defined as the curl of the velocity, which is

$$\bar{\omega} = \nabla \times \bar{u} \tag{1.3}$$

Since the fluid flow is potential, it is irrotational inside and outside the cylinder, and is incompressible everywhere. Additionally, the condition of zero viscosity (inviscid flow) is imposed everywhere. Given these conditions, the following is true

$$\bar{\omega} = \nabla \times \bar{u} = (0,0,v_x - u_y) = \bar{0} \qquad \text{(vorticity is zero except on the cylinder)} \tag{1.3}$$

which implies that

$$\frac{\partial v}{\partial x} = \frac{\partial u}{\partial y} \tag{1.4}$$

and since the fluid is incompressible, divergence is zero:

$$\frac{\partial u}{\partial x} = -\frac{\partial v}{\partial y} \tag{1.5}$$

Equations (1.4) and (1.5) are known as the Cauchy-Riemann equations. Equation (1.2) must satisfy the Cauchy-Riemann equations and is therefore analytic.

2. The Vortex Sheet Model

A vortex sheet is a zero-thickness model for a shear layer in an incompressible and inviscid fluid. The velocity is therefore discontinuous across the vortex sheet. See Figs. 2.1 and 2.2. Let the fluid velocities on opposite sides of the vortex sheet be either U^+ or U^-. The jump can then be described as a step function with magnitude (U^- - U^+). The vorticity along the vortex sheet is then defined as

$$\omega = (U^- - U^+)\delta(y) \tag{2.1}$$

where $\delta(y)$ represents the dirac delta function - the derivative of the step function. A primary goal of setting up this problem is to determine the velocity jump everywhere along the vortex sheets such that the potential flow described in Section 1 is induced. This velocity jump will be defined as

$$\sigma(\alpha) = (U^- - U^+)(\alpha) \qquad \text{which is the strength of the vortex sheet} \tag{2.2}$$

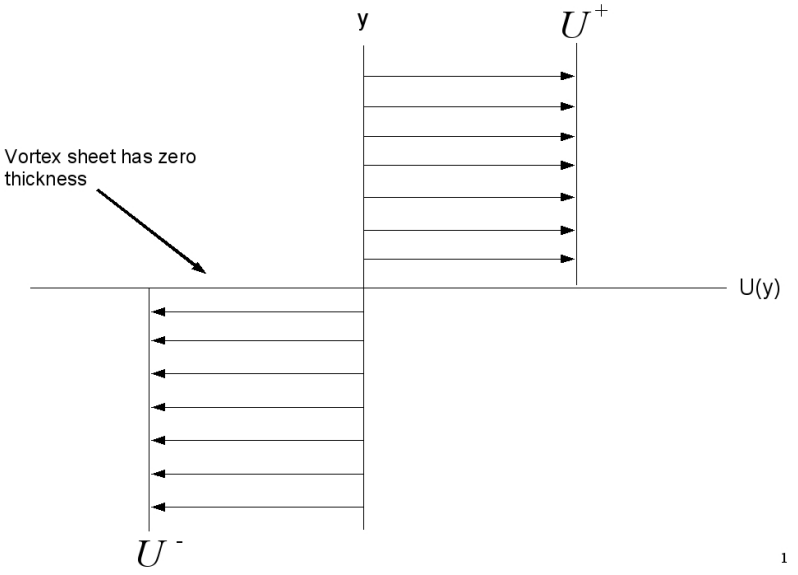

Fig. 2.1. The vortex sheet is a velocity jump of zero thickness. Although U- is shown here, the fluid is stationary inside the cylindrical vortex sheets described in this problem.

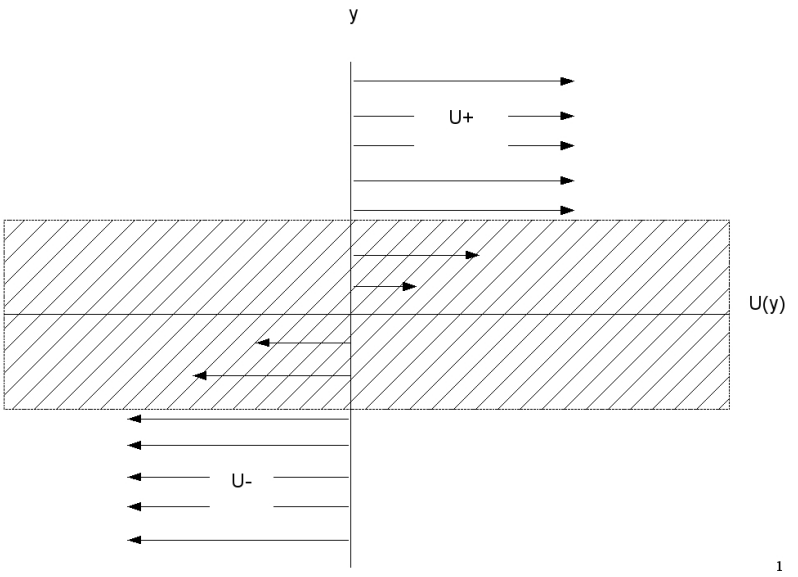

Fig. 2.2. A shear layer (above) can be approximated by a vortex sheet.

3. Paramaterization

Let *R* represent the radius of the cylinder, and *D* represent the distance between the center of each cylinder and the x-axis. In the cartesian coordinate system of (x,y), we can then parameterize each sheet by

$$x(\alpha), \quad y(\alpha) \tag{3.1}$$

Let us define the circulation parameter Γ(α) such that

$$\frac{d\Gamma}{ds} = \sigma(s) \tag{3.2}$$

where s is the arclength along the vortex sheet. The parameter σ is the jump in the velocity across the vortex sheet, as defined by (2.2).

The vortex sheet is discretized into evenly-spaced point-vortex elements. The following parameterization is used:

$$x(\alpha_j) = R\cos(\alpha_j) \qquad y(\alpha_j) = \frac{D}{R} + R\sin(\alpha_j) \qquad \alpha_j = \frac{2\pi j}{N} \tag{3.3}$$

where j = 0, ..., N-1. See Fig. 3.1.

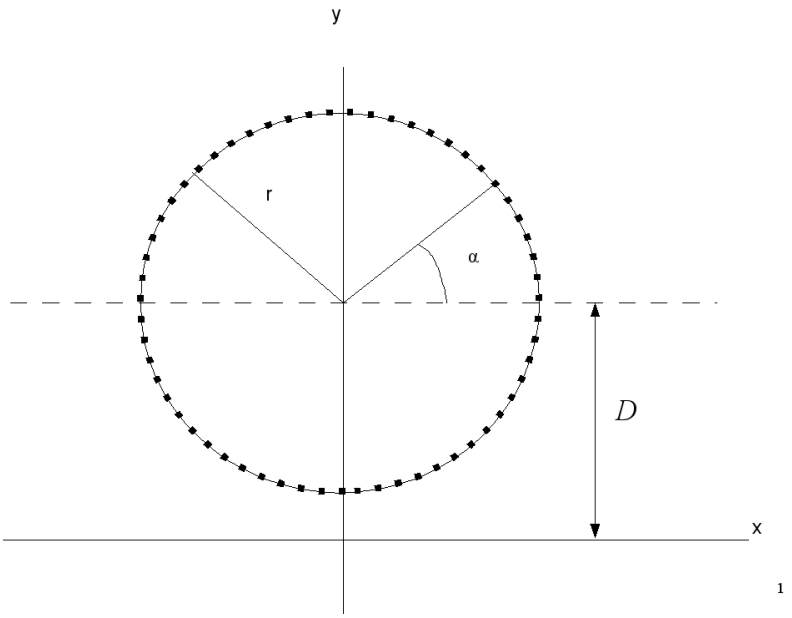

Fig. 3.1 Parameterization and discretization of vortex sheet. The second cylinder is not shown, but is a mirror image across the x-axis.

4. Evolution Equation

The general stream function at (x,y) due to one point vortex at (x̃,ỹ), excluding all others is

$$\psi(x,y,\tilde{x},\tilde{y})=\frac{-\Gamma_j}{4\pi}\log[(x-\tilde{x})^2+(y-\tilde{y})^2] \tag{4.1}$$

The velocity field at (x,y) induced by one point vortex at (x̃,ỹ), excluding all others, is given by

$$(u,v)=(\partial_y\psi,-\partial_x\psi)=\left(\frac{-\Gamma_j}{2\pi}\left(\frac{y-\tilde{y}}{r^2}\right),\frac{\Gamma_j}{2\pi}\left(\frac{x-\tilde{x}}{r^2}\right)\right) \quad \text{where } r^2=(x-\tilde{x})^2+(y-\tilde{y})^2 \tag{4.2}$$

The superposition of infinitely many point-vortex elements gives

$$\begin{aligned} u(x,y)&=\frac{1}{2\pi}PV\int_0^{2\pi}\frac{-(y-\tilde{y})\Gamma'(\alpha)}{(x-\tilde{x})^2+(y-\tilde{y})^2}d\alpha-\int_0^{2\pi}\frac{-(y+\tilde{y})\Gamma'(\alpha)}{(x-\tilde{x})^2+(y+\tilde{y})^2}d\alpha \\ v(x,y)&=\frac{1}{2\pi}PV\int_0^{2\pi}\frac{(x-\tilde{x})\Gamma'(\alpha)}{(x-\tilde{x})^2+(y-\tilde{y})^2}d\alpha-\int_0^{2\pi}\frac{(x-\tilde{x})\Gamma'(\alpha)}{(x-\tilde{x})^2+(y+\tilde{y})^2}d\alpha \end{aligned} \tag{4.3}$$

where *PV* denotes a principal value integral.

To approximate the total velocity induced by the vortex sheets, the effect of N point vortices is superimposed with the parameterization given in Section 3. The velocity at the *j*th point on the top sheet due to contributions from the *k*th vortices on one sheet above and one sheet below the x-axis is given by

$$\begin{aligned} u(x_j,y_j)&=\frac{-1}{2\pi}\sum_{k=0,k\neq j}^{N-1}\frac{y_j-y_k}{(x_j-x_k)^2+(y_j-y_k)^2}\sigma_k\Delta s+\frac{1}{2\pi}\sum_{k=0}^{N-1}\frac{y_j+y_k}{(x_j-x_k)^2+(y_j+y_k)^2}\sigma_k\Delta s \\ v(x_j,y_j)&=\frac{1}{2\pi}\sum_{k=0,k\neq j}^{N-1}\frac{x_j-x_k}{(x_j-x_k)^2+(y_j-y_k)^2}\sigma_k\Delta s-\frac{1}{2\pi}\sum_{k=0}^{N-1}\frac{x_j-x_k}{(x_j-x_k)^2+(y_j+y_k)^2}\sigma_k\Delta s \end{aligned} \tag{4.4}$$

Since σ_k will be used in the following sections to compute the initial condition, $\sigma_k\Delta s$ has been substituted for $d\Gamma$ since $\sigma=\frac{d\Gamma}{ds}$ and $ds=\frac{2\pi}{N}$ is constant.

To complete the initial conditions, the unknown sheet strength $\sigma(\alpha)$ will be found in Section 6, and equations (3.3) will be restated in dimensionless quantities in the following Section 5.

5. Nondimensionalization

In order to remove units, this problem is nondimensionalized. The following dimensionless quantities (denoted by *) are introduced:

$$x^* = \frac{x}{R} \quad \Rightarrow \quad R\,x^* = x \text{ and } \frac{dx}{dx^*} = R, \qquad y^* = \frac{y}{R} \quad \Rightarrow \quad R\,y^* = y \text{ and } \frac{dy}{dy^*} = R \tag{5.3a}$$

$$\Gamma^* = \frac{\Gamma}{RU} \quad \Rightarrow \quad RU\,\Gamma^* = \Gamma \quad \Rightarrow \quad RU\,d\Gamma^* = d\Gamma \tag{5.3b}$$

$$\tilde{x}^* = \frac{\tilde{x}}{R} \quad \Rightarrow \quad R\,\tilde{x}^* = \tilde{x}, \qquad \tilde{y}^* = \frac{\tilde{y}}{R} \quad \Rightarrow \quad R\,\tilde{y}^* = \tilde{y} \tag{5.3c}$$

$$t^* = \frac{U}{R}t \quad \Rightarrow \quad \frac{dt^*}{dt} = \frac{U}{R} \tag{5.3d}$$

So,

$$\begin{aligned} R\,x^* &= x(\alpha,t) = R\cos\alpha \quad \Rightarrow \quad x^* = \cos\alpha, \\ R\,y^* &= y(\alpha,t) = D + R\sin\alpha \quad \Rightarrow \quad y^* = \frac{D}{R} + \sin\alpha \end{aligned} \tag{5.4}$$

Then using

$$\frac{dx(\alpha,t)}{dt} = \frac{dx}{dx^*}\frac{dx^*}{dt} = R\frac{dx^*}{dt} = R\frac{dx^*}{dt^*}\frac{dt^*}{dt} = R\frac{U}{R}\frac{dx^*}{dt^*} = U\frac{dx^*}{dt^*} \tag{5.5}$$

it follows that

$$\frac{dx^*}{dt^*} = \frac{1}{U}\left[U\frac{dx^*}{dt^*}\right] = \frac{1}{U}\frac{dx(\alpha,t)}{dt} = \frac{1}{U}\left[\frac{-1}{2\pi}\int_0^{2\pi}\left[\frac{y-\tilde{y}}{(x-\tilde{x})^2+(y-\tilde{y})^2}\right]\frac{d\Gamma^*}{d\tilde{\alpha}}\,d\tilde{\alpha} + \frac{1}{2\pi}\int_0^{2\pi}\left[\frac{y+\tilde{y}}{(x-\tilde{x})^2+(y+\tilde{y})^2}\right]\frac{d\Gamma^*}{d\tilde{\alpha}}\,d\tilde{\alpha}\right] \tag{5.6}$$

and

$$\frac{dx^*}{dt^*} = \frac{1}{2\pi U}\int_0^{2\pi}\left[-\frac{Ry^*-R\tilde{y}^*}{(Rx^*-R\tilde{x}^*)^2+(Ry^*-R\tilde{y}^*)^2} + \frac{Ry^*+R\tilde{y}^*}{(Rx^*-R\tilde{x}^*)^2+(Ry^*+R\tilde{y}^*)^2}\right]\frac{RU\,d\Gamma^*}{d\tilde{\alpha}}\,d\tilde{\alpha} \tag{5.7}$$

Finally, after the R and U terms cancel,

$$\frac{dx^*}{dt^*} = \frac{1}{2\pi}\int_0^{2\pi}\left[-\frac{y^*-\tilde{y}^*}{(x^*-\tilde{x}^*)^2+(y^*-\tilde{y}^*)^2} + \frac{y^*+\tilde{y}^*}{(x^*-\tilde{x}^*)^2+(y^*+\tilde{y}^*)^2}\right]\frac{d\Gamma^*}{d\tilde{\alpha}}\,d\tilde{\alpha} \tag{5.8}$$

The process is similar for $\frac{dy^*}{dt^*}$, yielding

$$\frac{dy^*}{dt^*} = \frac{1}{2\pi}\int_0^{2\pi}\left[\frac{x^*-\tilde{x}^*}{(x^*-\tilde{x}^*)^2+(y^*-\tilde{y}^*)^2}-\frac{x^*-\tilde{x}^*}{(x^*-\tilde{x}^*)^2+(y^*+\tilde{y}^*)^2}\right]\frac{d\Gamma^*}{d\tilde{\alpha}}d\tilde{\alpha} \tag{5.9}$$

Therefore, the equations that govern the motion of the vortex sheet do not change as the variables are nondimensionalized. Equations (3.3) can now be re-defined in dimensionless quantities as

$$x(\alpha_j)=\cos(\alpha_j) \qquad y(\alpha_j)=\mu+\sin(\alpha_j) \qquad \text{where} \quad \mu=\frac{D}{R} \quad \text{and} \quad \alpha_j=\frac{2\pi j}{N} \tag{5.10}$$

This simplification yields one quantity, namely μ, that is varied in order to study the effect the vortex sheet have on one another. When μ = 1, the cylinders are touching, and when μ = ∞, the cylinders have no effect on one another, reducing to the single cylinder case.

6. Point-Vortex Strengths

The only missing part of the initial condition is the vortex sheet strength *σ(α)*. First, let us restate the evolution equations (4.4) and subtract from them the background velocity - prescribed as $U^\infty = 1$ and $V^\infty = 0$ at infinite distance - that the cylinders are "inserted" into:

$$\begin{aligned} u(x_j,y_j)&=\frac{-1}{2\pi}\sum_{k=0,k\neq j}^{N-1}\frac{y_j-y_k}{(x_j-x_k)^2+(y_j-y_k)^2}\sigma_k\Delta s+\frac{1}{2\pi}\sum_{k=0}^{N-1}\frac{y_j+y_k}{(x_j-x_k)^2+(y_j+y_k)^2}\sigma_k\Delta s-U^\infty \\ v(x_j,y_j)&=\frac{1}{2\pi}\sum_{k=0,k\neq j}^{N-1}\frac{x_j-x_k}{(x_j-x_k)^2+(y_j-y_k)^2}\sigma_k\Delta s-\frac{1}{2\pi}\sum_{k=0}^{N-1}\frac{x_j-x_k}{(x_j-x_k)^2+(y_j+y_k)^2}\sigma_k\Delta s-V^\infty \end{aligned} \tag{6.1}$$

At the vortex sheets, the exterior fluid velocity is entirely tangential to the surface. Therefore, it follows that

$$\boldsymbol{u}(\alpha_j^m)\cdot\boldsymbol{n}(\alpha_j^m) = 0 \tag{6.2}$$

where the superscript *m* refers to the normal vectors at midpoints between vortices. See Fig. 6.1. This results in the linear system

$$\boldsymbol{A\sigma=b} \tag{6.3}$$

where $\boldsymbol{A\sigma}$ represents equations in (6.1) without the background velocity, and $\boldsymbol{b}$ is given by

$$b_j=U^\infty\cos(\alpha_j^m) \tag{6.4}$$

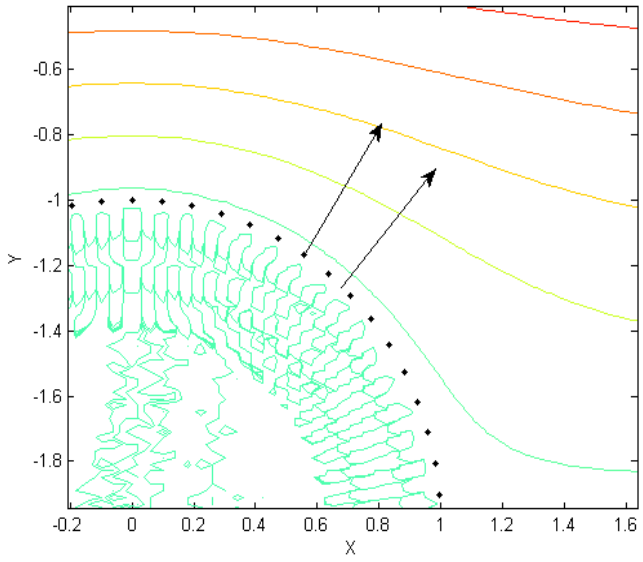

Fig. 6.1.

Equation (6.3) was first solved using the normal vectors at the actual vortex points. This resulted in erroneous results with the condition number for $\boldsymbol{A}$, which is defined as

$$\kappa(\alpha)=\|\boldsymbol{A}^{-1}\|\cdot\|\boldsymbol{A}\| \tag{6.4}$$

on the order of 10^{15} to 10^{17} for N = 16, 32, 64, 128, and 256. This indicates an ill-posed problem. See Fig. 6.2.

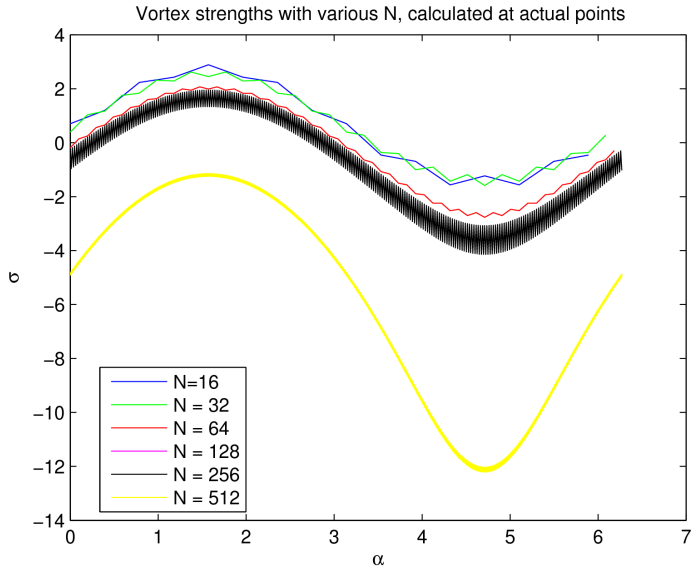

Fig. 6.2. Erroneous results for $\sigma(\alpha)$ when normal vectors at actual points are used.

When the linear system (6.3) is is then solved using normal vectors at the midpoints, the condition number, κ, remains large (~ 10^{15}), and the following results (Fig. 6.3) seem to oscillate around the desired solution for $\sigma(\alpha)$ as N is increased.

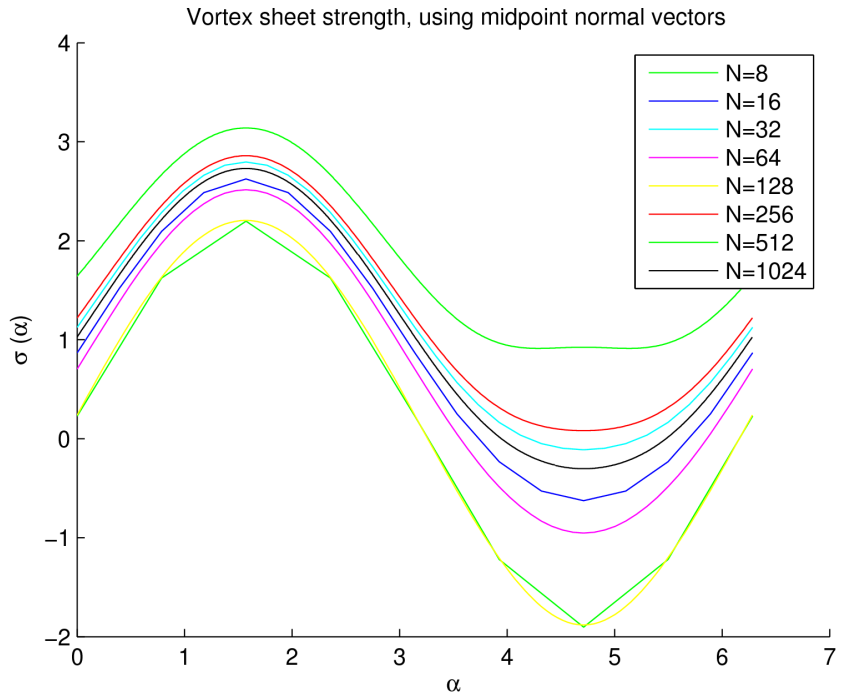

Fig. 6.3.

To correct these errors, the condition that total circulation equals zero is imposed:

$$\Gamma_T = \frac{2\pi}{N}\sum_{j=1}^{N}\sigma(\alpha_j) = 0 \qquad (6.4)$$

This condition is is certainly the case with a single cylindrical vortex sheet, but is not analytically known for two cylindrical vortex sheets. Nevertheless, it is applied to (6.3), results in the following modified linear system:

$$\begin{bmatrix} A_{11} & A_{12} & \cdots & A_{1n} \\ A_{21} & & & A_{2N} \\ \vdots & & & \vdots \\ A_{N1} & A_{n2} & \cdots & A_{NN} \\ \Delta s & \Delta s & \cdots & \Delta s \end{bmatrix} \begin{bmatrix} \sigma_1 \\ \sigma_2 \\ \vdots \\ \sigma_N \end{bmatrix} = \begin{bmatrix} b_1 \\ b_2 \\ \vdots \\ b_N \\ 0 \end{bmatrix} \qquad \text{where} \quad \Delta s = \frac{2\pi}{N} \qquad (6.5)$$

When the above equations - now an overdetermined system - are solved in the least-squares sense, the result is exponentially accurate convergence for $\sigma(\alpha)$, and very small residuals $\boldsymbol{A\sigma - b}$. The error seen in Fig. 6.4 was computed by using a fine mesh with N=1024, and comparing with the results of mesh sizes N=32, 64, 128, 256, and 512. It was also determined that as μ was made large, the

computed vortex strengths converge to the analytical solution for the single cylinder case where $\sigma(\alpha) = \sin(\alpha)$. See Fig. 6.5.

Using the computed point-vortex strengths, the streamlines seen in Fig. 6.6 were computed and superimposed on the initial position of the discretized vortex sheets.

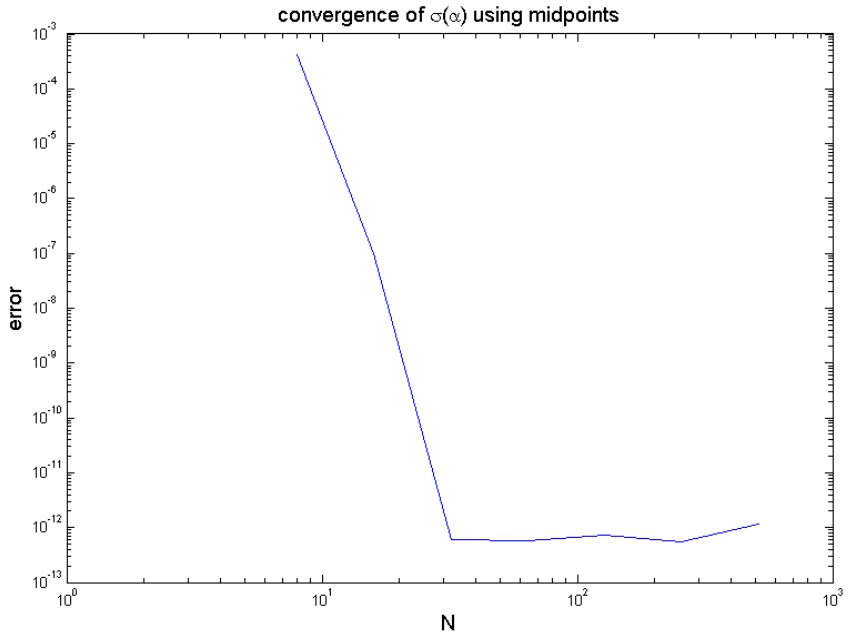

Fig. 6.4. Convergence of vortex sheet strengths as N increases, with total circulation of zero imposed.

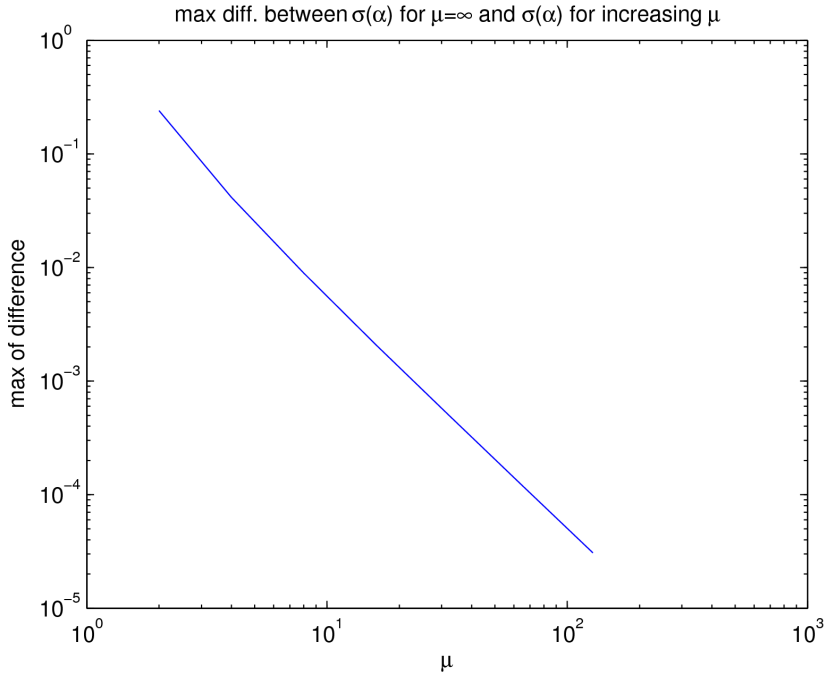

Fig. 6.5. Verification that $\sigma(\alpha)$ for two-cylinder case approaches $\sigma(\alpha)$ for single cylinder case ($\mu = \infty$) as μ becomes large.

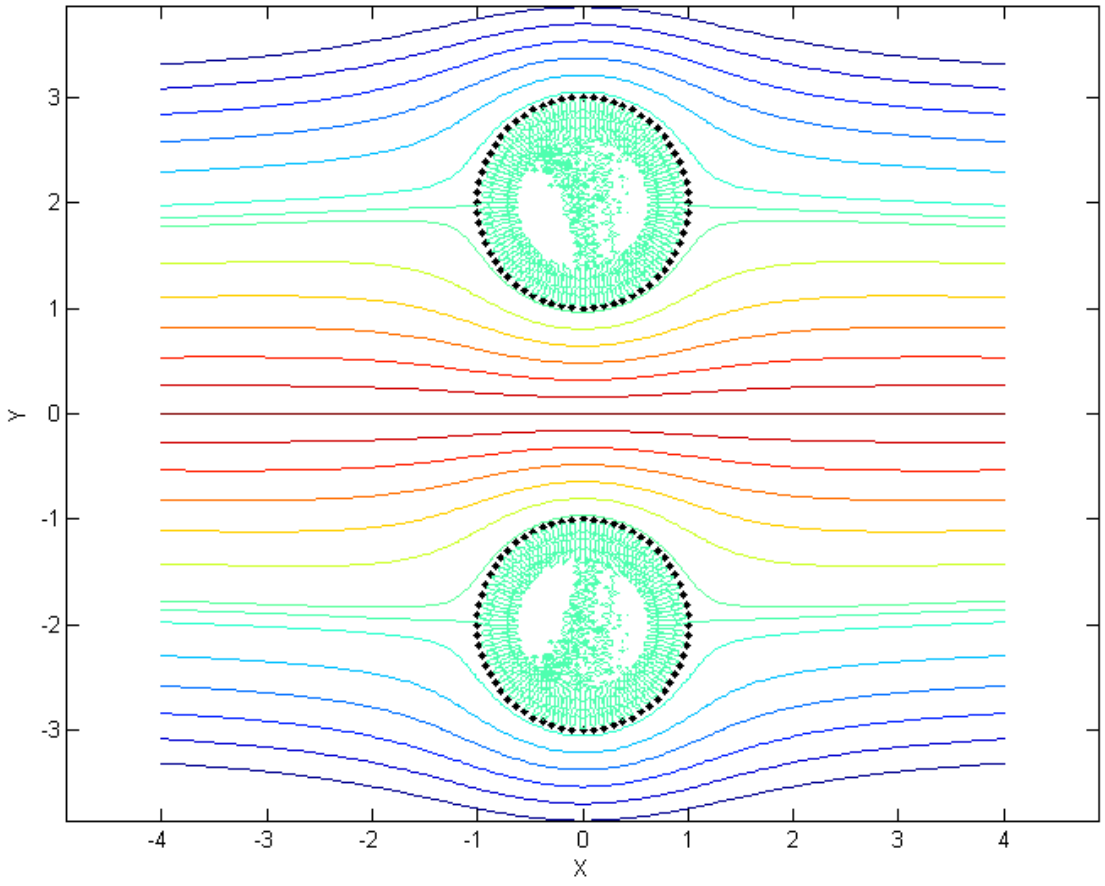

Fig. 6.5. Streamlines that represent the potential flow around the cylinders. The fluid is stationary inside the cylinders. Note the numerical noise in the computation of the position of the zero streamline.

7. Numerical Instability

As the number of point vortices is increased, numerical instability leads to a lack of convergence, contradicting what may be expected. Furthermore, due to singularity formation from Kelvin-Helmholtz instability, the results are erroneous past a critical time. To compute the evolution of the vortex sheets, this problem must proceed in one of two directions: (1) Adding a regularization parameter to the first denominator of (4.4) to allow computation past the critical time, or (2) Increasing the accuracy of the computation using a correction factor to (4.4) and reducing noise by filtering the Fourier coefficients, without evolving past the critical time. These two methods are described in the following sections.

8. Regularized Case

In order to evolve past the critical time of singularity formation, a regularization parameter δ^2 is added to the first denominator of (4.4), thus preventing irregular point vortex motion. The problem *is* changed. However, as $\delta \to 0$ and the mesh is refined, the convergence to the actual problem can be explored. The discretized equations for the point-vortex motion are given with the regularization parameter δ^2:

$$u(x_j, y_j) = \frac{-1}{2\pi} \sum_{k=0}^{N-1} \frac{y_j - y_k}{(x_j - x_k)^2 + (y_j - y_k)^2 + \delta^2} \sigma_k \Delta s + \frac{1}{2\pi} \sum_{k=0}^{N-1} \frac{y_j + y_k}{(x_j - x_k)^2 + (y_j + y_k)^2} \sigma_k \Delta s$$

$$v(x_j, y_j) = \frac{1}{2\pi} \sum_{k=0}^{N-1} \frac{x_j - x_k}{(x_j - x_k)^2 + (y_j - y_k)^2 + \delta^2} \sigma_k \Delta s - \frac{1}{2\pi} \sum_{k=0}^{N-1} \frac{x_j - x_k}{(x_j - x_k)^2 + (y_j + y_k)^2} \sigma_k \Delta s \qquad (8.1)$$

These equations are then solved using the fourth-order Runge Kutta method and the initial condition given by (5.10). See Fig.8.1 for preliminary results. This computation was performed with N=1024. As longer computation times are used, and the sheets are placed closer together, it will be necessary to insert points to maintain sufficient accuracy.

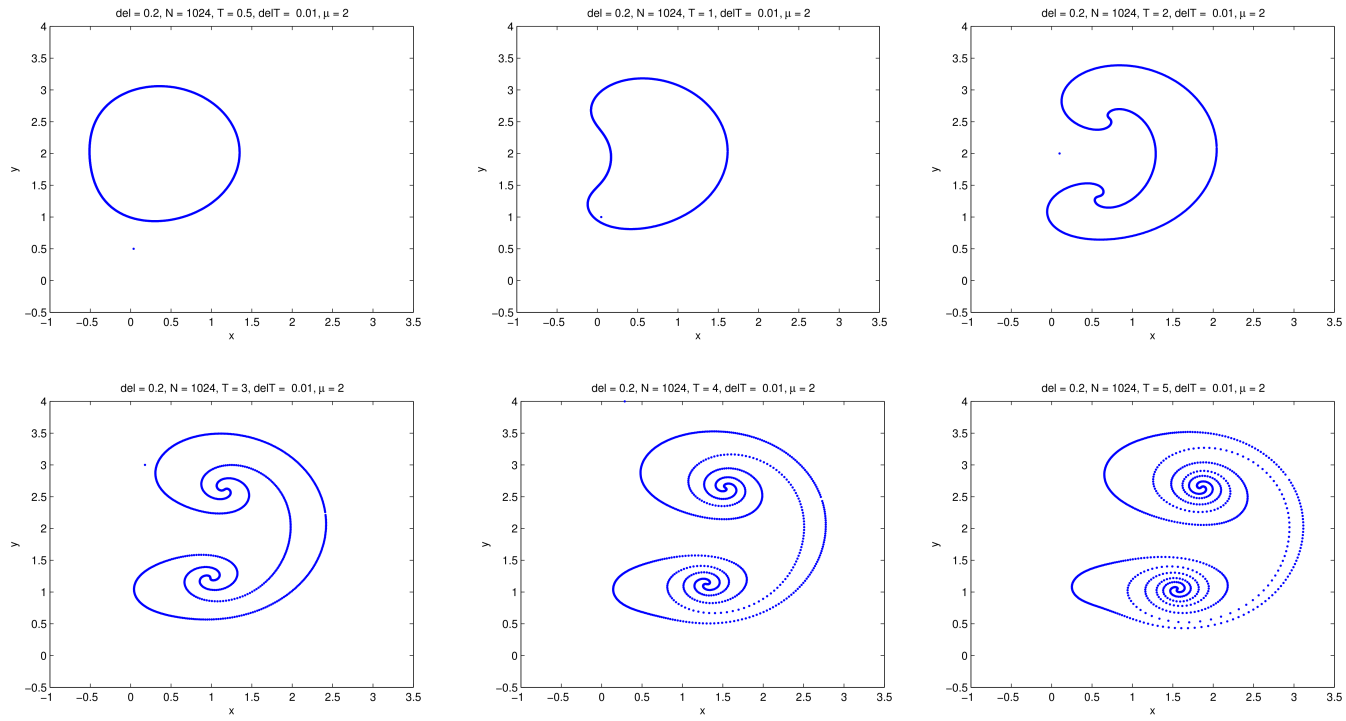

Fig. 8.1. Computed solution of upper vorte sheet up to time t = 5.0 with regularization parameter.

9. Singular Case

The evolution equations (4.3) include principal value integrals which are necessary to exclude the velocity contribution of nearby portions of the vortex sheet. Since equations (4.4) use the trapezoid rule, this will result in a loss of accuracy. Convergence of O(1/N) is observed as seen in Fig. 9.1. The second integrals in each of (4.3), which represent contributions from the bottom cylinder are computed with exponential accuracy (with respect to mesh size) using the trapezoid rule. In order to achieve exponential accuracy for the principal value integrals, a correction factor $\tilde{G}(\alpha)$ is added to (4.3) by using a Taylor series about $\alpha = \alpha_j$. First, let

$$G^u(\alpha)=\frac{(y_j-y(\alpha))\,\Gamma'(\alpha)\,d\alpha}{(x_j-x(\alpha))^2+(y_j-y(\alpha))^2} \qquad \text{which is the integrand of the u component of (4.3)} \qquad (9.1)$$

where

$$h = (\alpha-\alpha_j), \quad x_j = x(\alpha_j), \quad y_j = y(\alpha_j), \quad \text{and} \quad \Gamma_j=\Gamma(\alpha_j) \qquad (9.2)$$

Then

$$x_j-x(\alpha)=-x'_j h-\frac{x''_j}{2}h^2-O(h^3), \quad y_j-y(\alpha)=-y'_j h-\frac{y''_j}{2}h^2-O(h^3), \quad \text{and} \quad \Gamma'(\alpha)=\Gamma'_j+\Gamma''_j h+O(h^2) \qquad (9.3)$$

Now, expand $G^u(\alpha)$:

$$G^u(\alpha)=\frac{\left[-y'_j h-\frac{y''_j}{2}-O(h^3)\right]\left[\Gamma'_j+\Gamma''_j h+O(h^2)\right]}{(x'^2_j+y'^2_j)h^2+(x'_j x''_j+y'_j y''_j)h^3+O(h^4)} = \frac{\frac{-y_j\Gamma'_j}{h}-(\frac{y''_j}{2}\Gamma'_j+y'_j\Gamma''_j)+O(h)}{(x'^2_j+y'^2_j)+(x'_j x''_j+y'_j y''_j)h+O(h^2)} \qquad (9.4)$$

Let the following be the C_0^u term from the above Taylor series be the correction factor $\tilde{G}^u(\alpha)$:

$$C_0^u = \frac{1}{x'^2_j+y'^2_j}\left[\frac{-y'_j\Gamma'_j(x'_j x''_j+y'_j y''_j)}{x'^2_j+y'^2_j}-\left(\frac{y''_j}{2}\Gamma'_j+y'_j\Gamma''_j\right)\right] \qquad (9.5)$$

The C_0^v term is derived similarly,

$$C_0^v = \frac{1}{x'^2_j+y'^2_j}\left[\frac{-x'_j\Gamma'_j(x'_j x''_j+y'_j y''_j)}{x'^2_j+y'^2_j}-\left(\frac{x''_j}{2}\Gamma'_j+x'_j\Gamma''_j\right)\right] \qquad (9.6)$$

These terms are then added to their respective components of (4.3) and (4.4), thus yielding exponential accuracy. The accuracy of the corrected upper contributions and lower contributions is given in Fig. 9.2. The corrected equations for the self-induced motion of the vortex sheet are then evolved through time using the fourth-order Runge Kutta method with the initial condition given by (5.10).

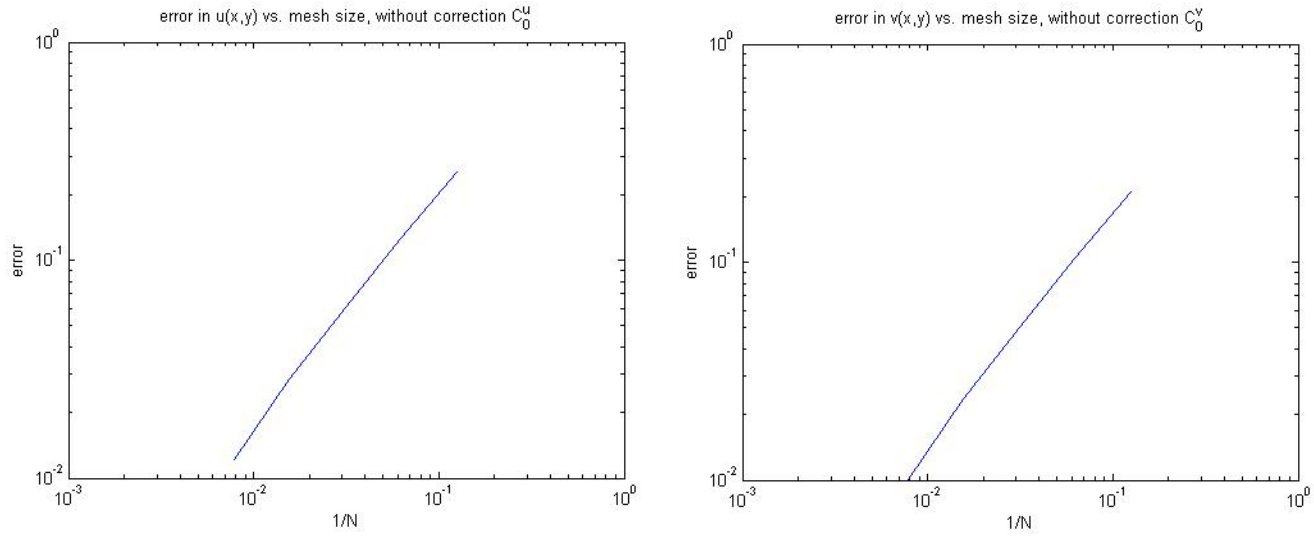

Figure 9.1. Convergence is of O(h) without correction factor.

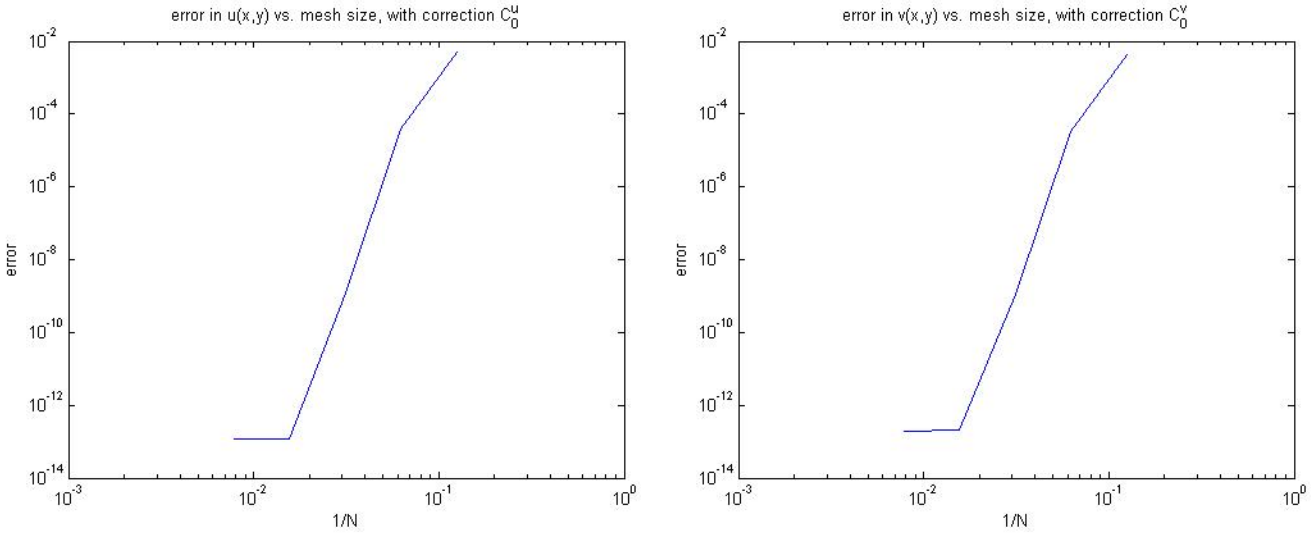

Fig. 9.2. The error drops to the level of roundoff error very quickly with correction factor.

In addition to the steps above, the Fourier coefficients of the point-vortex strengths below 8×10^{-15} were filtered out. The Fourier coefficients of the positions of the point-vortices below 10^{-12} were also filtered out at each timestep. This removes as much noise as possible due to roundoff error. However, as N is increased, less noise can be filtered out without removing meaningful data, and the use of a quadruple precision machine becomes necessary to achieve more accurate results. Some preliminary results for the singular case are shown in Fig. 9.3, up to time t = 0.5, with μ=2. This is the time when the first signs of singularity formation occur, and the evolution is stopped. The exact time of singularity formation, and its correlation with the geometric conditions is a topic saved for future analysis of the results.

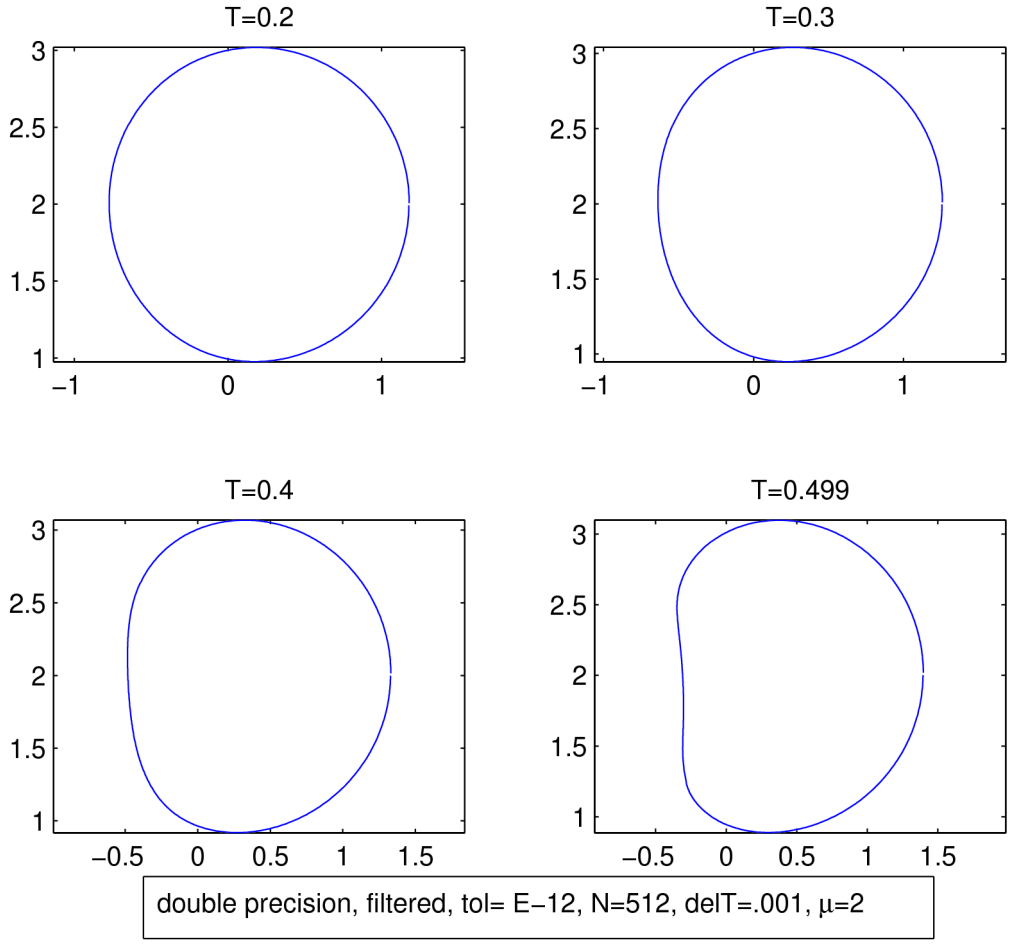

Fig. 9.3. The evolution of the upper cylindrical vortex sheet, up to critical time of singularity formation.

10. Conclusions

When two hollow cylinders are placed next to each other in potential flow – a physical analogy to the initial condition of two cylindrical vortex sheets – there is no known analytical solution for the stream function. As a result, the initial vortex sheet strength has been solved numerically to complete the initial condition. Due to the nature of the numerical instability of the evolution equations for vortex sheets, high accuracy is required for the initial condition. This requires care in computing the initial vortex sheet strength. Once the linear system for the point-vortex strengths was properly posed, and the expected circulation conditions were imposed, a solution accurate to 10^{-12} was achieved. Furthermore, correction factors were required for the non-regularized evolution equations to achieve sufficient accuracy. The initial condition and evolution equations that have been presented can be used, along with filtering of noise and regularization, to study the motion and behavior of dual cylindrical vortex sheets in detail.

References

1. M.J. Ablowitz and A.S. Fokas, *Complex Variables: Introduction and Applications*, 2nd ed. (Cambridge University Press, Cambridge, UK, 2003)
2. A.J. Chorin and J.E. Marsden, *A Mathematical Introduction to Fluid Mechanics*, 3rd ed. (Springer-Verlag, New York, 2000)
3. H.F. Davis and A.D. Snider, *Introduction to Vector Analysis,* 7th ed. (Hawkes Publishing, Tallahasse, FL, 2000)
4. R. Krasny, Desingularization of Periodic Vortex Sheet Roll-Up, *Journal of Computational Physics*, vol. 65, No. 2, 292-313 (1986).
5. R. Krasny, A study of singularity formation in a vortex sheet by the point-vortex approximation, *J. Fluid Mech.* vol. 167, 65-93 (1986).
6. M. Nitsche, Math 471: Introduction to Scientific Computing (UNM Course Notes, 2006)
7. M. Nitsche, Self-similar shedding of vortex rings, *J. Fluid Mech.*, vol. 435, 397-407 (2001).
8. M. Nitsche, Singularity Formation in a Cylindrical and a Spherical Vortex Sheet, *Journal of Computational Physics*, vol. 173, 208-230 (2001).